Supporting Information for "Probing the Martian atmospheric boundary layer using impact-generated seismo-acoustic signals"

Marouchka Froment[1,2,3], Zongbo Xu[1], Philippe H. Lognonné[1], Carène Larmat[2], Raphael F. Garcia[4], Mélanie Drilleau[4], Brent G Delbridge[2], Aymeric Spiga[5], Taichi Kawamura[1], Éric Beucler[6,7]

[1]Université Paris Cité, Institut de physique du globe de Paris, CNRS, F-75005 Paris, France

[2]Earth and Environmental Sciences Division, Los Alamos National Laboratory, Los Alamos, NM 87545, USA

[3]NORSAR, Kjeller, Norway

[4]Institut Supérieur de l'Aéronautique et de l'Espace (ISAE-SUPAERO), Université de Toulouse, 31400 Toulouse, France

[5]Laboratoire de Météorologie Dynamique/Institut Pierre-Simon Laplace (LMD/IPSL), CNRS, Sorbonne Université, Paris, France

[6]Nantes Université, Université Angers, Le Mans Université, CNRS, UMR 6112, Laboratoire de Planétologie et Géosciences, F-44000 Nantes, France

[7]Nantes Université, UGE, Univ Angers, CNAM, CNRS, UAR 3281, Observatoire des sciences de l'univers Nantes Atlantique, F-44000 Nantes, France

InSight Contribution Number 265. LA-UR-23-33646.

Contents of this file

Corresponding author: M. Froment (mfroment@ipgp.fr, mfroment@lanl.gov)

Introduction

This Supporting Information presents the method of measurement of group velocity from SEIS signals, parametric studies of the group velocity calculation, tests of the Markov-chain Monte Carlo (McMC) method used in this study, model statistics, as well as maps and profiles of the wind and sound speed conditions predicted by the Mars Climate Database (MCD) (Millour et al., 2015, 2018) during events S0981c, S0986c and S1034a of the InSight mission. Spatial variations of wind and sound speed over the MCD interpolation grid are used to estimate an uncertainty for these profiles.

1. Group velocity measurement

Group velocities are measured as in Garcia et al. (2022), following the method of Gaudot et al. (2021). A dispersion plot is obtained using narrow Gaussian band-pass filters in multiple frequency bands and the source-receiver distance. The result is converted into a probability density function (PDF), in the sense that for each frequency bin, the integral over the velocity domain is equal to 1. At each frequency, the peak of PDF gives us a group velocity measurement, and the distance between the peak and the point of maximum gradient around the peak gives the uncertainty of the measurement.

2. Parametric study - forward model

The sensitivity of the calculated group velocity to discretization is shown in Fig. S1. The atmospheric sound speed profile predicted by the MCD (version 5.3) around InSight during S0986c is used to calculate the group velocity for a smoothly-varying model. The same calculation for two rough, 4-layer and 8-layer discretizations are compared. Below 2 Hz, the group velocity curve of smoothly-varying atmospheric profiles such as provided by MCD can be well reproduced by a layered profile with a low number N of layers, typically less than 10.

A parametric study is performed to determine the sensitivity of v_g to variations in effective sound speed and density. The 4-layer model of Fig. S1 is used as a reference, and is perturbed at different altitudes. Fig. S2 show that v_g is more sensitive to variations in effective sound speed than in density in the Martian atmosphere. Small perturbations in α_{eff} close to the surface result in large changes of v_g.

3. Test of the McMC method

Fig. S3 shows the influence of the number of layers in the atmospheric models on the mean misfit achieved by the inversion. It shows that increasing the number of layers from 1 to 4 significantly improves the misfit of the inverted models. However, no notable improvement is seen beyond this number. The atmosphere is consequently represented with 4 layers in all subsequent inversions.

Fig. S4 shows a synthetic inversion test. To conduct this test, the 4-layer model of Fig. S1 is used as an input. This effective sound speed profile is based on the MCD estimate for event S0986c (Fig. S4, left). A synthetic group velocity curve is calculated from this input model, and its uncertainty is considered to be the same as observed during event S0986c. Both are passed to the McMC inversion. The Probability Density Function (PDF) of effective sound speed profiles retrieved by the inversion shows a good match with the input model, within ±5 m/s. The group velocity curves retrieved from the posterior distribution also match the input model.

The performance and convergence of the inversion is also tested. By definition of a Markov chain, models $\boldsymbol{m}$ sampled from the posterior distribution with the McMC method are inherently correlated with each other. An important assessment of the quality of the inversion consist in measuring the amount of statistically significant samples within a chain. A chain requires a certain number of steps τ_c before it "forgets" its origin sample, i.e., before multiple portions of τ_c samples become similar to each other. τ_c is equivalent to the auto-correlation time of a chain, which writes based on Foreman-Mackey et al. (2013):

$$\tau_c(N) = 1 + 2\sum_{\tau=1}^{N} \frac{\hat{C}_f(\tau)}{\hat{C}_f(0)}, \tag{1}$$

with $\hat{C}_f(\tau)$ the auto-correlation function with lag τ, given by:

$$\hat{C}_f(\tau) = \frac{1}{N-\tau}\sum_{n=1}^{N-\tau}(f_n - \mu_f)(f_{n+\tau} - \mu_f). \tag{2}$$

f_n is the content of a chain of length n and $\mu_f = \frac{1}{N}\sum_{n=1}^{N} f_n$ is the mean value of the total chain. In practice, τ_c can be calculated progressively during a McMC run and converges when the simulation has sufficiently explored the posterior space. The posterior distribution can be considered sufficiently sampled for $N \approx 1000\tau_c$. Fig. S5 shows that our McMC method converges after about 2×10^5 iterations.

The calculation of group velocity curves from a layered model requires the resolution of a Newton-Raphson algorithm. With our implementation of the parallel tempering technique, each iteration takes about 0.3 s for a 4-layer model, 10 temperature levels and $\sim$ 50 values in frequency. The minimum simulation time for a chain to converge is therefore about four days with an Intel Xeon Platinum 8268 CPU (2.90GHz).

4. Prior and posterior distributions

As in Fig. 2 of the main text, Fig. S6 shows 100 group and phase velocity curves calculated from the posterior distribution of atmospheric models for events S0986c and S1034a, compared to the measured group velocity curve.

Fig. S7 shows the prior PDF of effective sound speed and estimated wind speed, using 50,000 models drawn from within the prior bounds. Probabilities shown in Figs. 2 and 3. of the main text can be compared to the prior probabilities.

Similarly, Fig. S8 shows histogram of some model parameters in the posterior and prior distributions. The altitude of each layer of the atmospheric models is displayed in the first column. The histograms show that the inversion places layers, and therefore transitions in effective sound speed, mostly below 500 m altitude, which correspond to the boundary layer of Mars. This distribution is different from the prior distribution, which confirms that this behavior is constrained by the group velocity data. In the middle column, the effective sound speed at the surface level (α_0) also has a well-defined distribution in the posterior, which is narrower than the prior. On the other hand, the effective sound speed in the halfspace (α_4), is well constrained only for S0981c. For S0986c, the data places a lower limit on α_4, but the distribution above 240 m/s is identical to the prior. Similarly, the posterior distribution of α_4 for S1034a has a Gaussian shape relatively similar to the prior, with a moderately narrower width. For both events, the data is not sufficient to constrain the upper-bound for effective sound speed at high altitude.

5. Weather conditions and local variations from the MCD

For events S0981c, S0986c and S1034a, the distance between the source and the receiver is smaller than the resolution of the Global Circulation Models (GCM) on which the MCD interpolation is based, which is 5.625° in longitude and 3.75° in latitude. The GCM also uses about 8 sampling points below 2000 m altitude (Forget et al., 2017).

The MCD profiles shown in the main text are calculated at InSight location. We choose to estimate an uncertainty for these profiles from the spatial variations of thermodynamic variables on a $\sim 5.6° \times 6°$ grid in longitude and latitude.

The spatial variation of wind at 50, 100 and 200 m altitude is represented on Fig. S9 along with the location of InSight and the crater. In all three cases, the wind shows a relatively stable dominant direction that is strongly in favor of infrasound propagation for events S0986c and S1034a, with winds of $\sim$ 10 m/s blowing from the source to InSight. This effect is less pronounced for S0981c.

We calculate vertical profiles of the thermodynamic sound speed $\alpha_T(z)$, the wind speed in the source-receiver direction $w_{\text{baz}}(z)$ and the effective sound speed $\alpha_{\text{eff}}(z)$, found on Fig. S10. Variations of ± 5 m/s in the effective sound speed are observed below 500 m altitude at the scale of the map of Fig. S9. The wind variations have a stronger influence on the effective sound speed profiles than the thermodynamic sound speed variations, which depend on local temperature. The minimum and maximum profiles are used to define the local uncertainty of the MCD estimate.

References

Foreman-Mackey, D., Hogg, D. W., Lang, D., & Goodman, J. (2013, March). emcee: The MCMC Hammer. *Publications of the Astronomical Society of the Pacific*, *125*(925), 306–312. (arXiv: 1202.3665) doi: 10.1086/670067

Forget, F., Millour, E., Vals, M., Zakharov, V., & Lewis, S. (2017, july). Mars climate database v5.3 detailed design document [Computer software manual].

Garcia, R. F., Daubar, I. J., Beucler, É., Posiolova, L. V., Collins, G. S., Lognonné, P., ... Banerdt, W. B. (2022, September). Newly formed craters on Mars located using seismic and acoustic wave data from InSight. *Nature Geoscience*, 1–7. doi: 10.1038/s41561-022-01014-0

Gaudot, I., Beucler, É., Mocquet, A., Drilleau, M., Haugmard, M., Bonnin, M., ... Leparoux, D. (2021, March). 3-D crustal VS model of western France and the surrounding regions using Monte Carlo inversion of seismic noise cross-correlation dispersion diagrams. *Geophysical Journal International*, *224*(3), 2173–2188. doi: 10.1093/gji/ggaa552

Millour, E., Forget, F., Spiga, A., Navarro, T., Madeleine, J. B., Montabone, L., ... MCD/GCM development Team (2015, October). The Mars Climate Database (MCD version 5.2). In *European Planetary Science Congress 2015* (Vol. EPSC2015, p. 438). Nantes, France.

Millour, E., Forget, F., Spiga, A., Vals, M., Zakharov, V., Montabone, L., ... Read, P. L. (2018). The Mars Climate Database (Version 5.3). In *Scientific Workshop: "From Mars Express to ExoMars"*. ESAC Madrid, Spain.

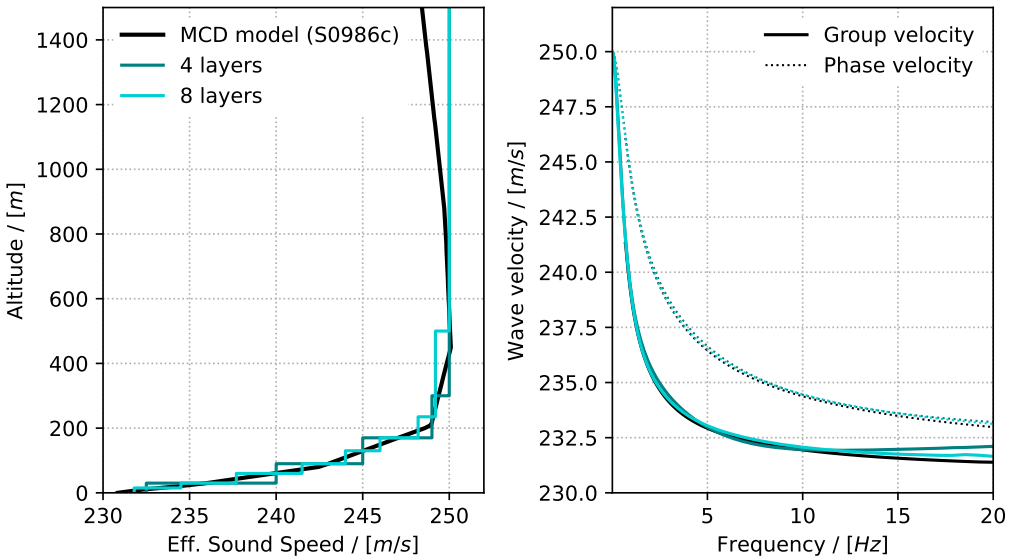

Figure S1. Sensitivity of the group velocity calculated with the propagator matrix method to the discretization of atmospheric profiles. (left) Effective sound speed profiles used in the test. The black curves represent MCD profiles at InSight location during event S0986c. A 4-layer and 8-layer discretization are also plotted. (right) Group and phase velocity calculated for each of the three models.

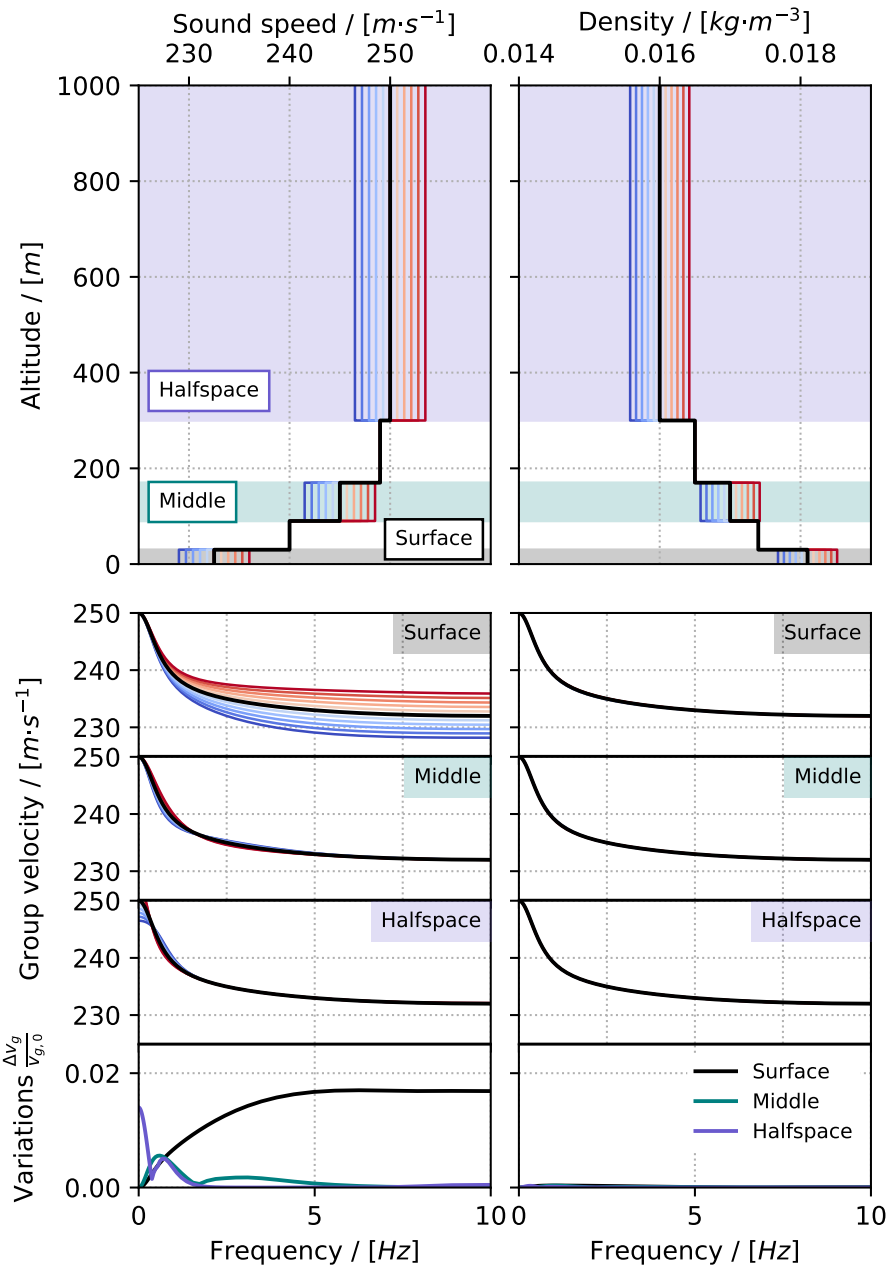

Figure S2. Sensitivity of the group velocity to changes in sound speed and density. For each group velocity curve shown in the middle plots, the value of either density or sound speed in one of the layers has been changed while all other layers remained identical to the 4-layer model of S1. The bottom plot shows variations of v_g with respect to the unperturbed model, for changes made in the halfspace (blue), the middle of the profile (green), and the surface (black). At low frequency, group velocity appears sensitive to changes in the halfspace, while most high-frequency variations are related to changes at surface level. Group velocities are more sensitive to variations in sound speed than in density.

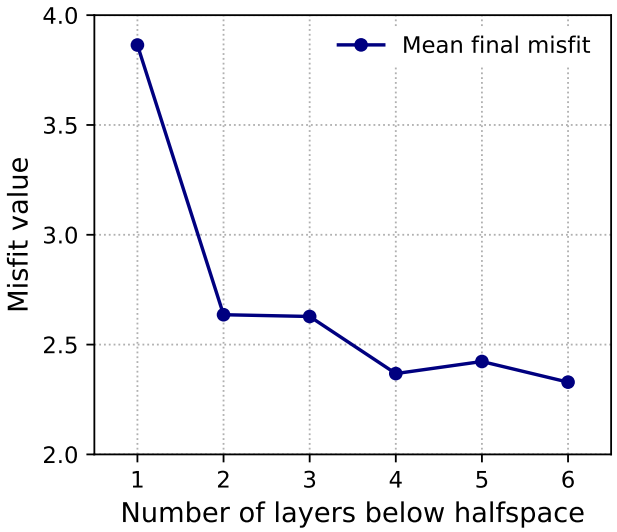

Figure S3. Mean misfit measured in the last $10,000$ iterations of the Markov chains as a function of the number of layers (below the halfspace) defining the atmospheric profiles.

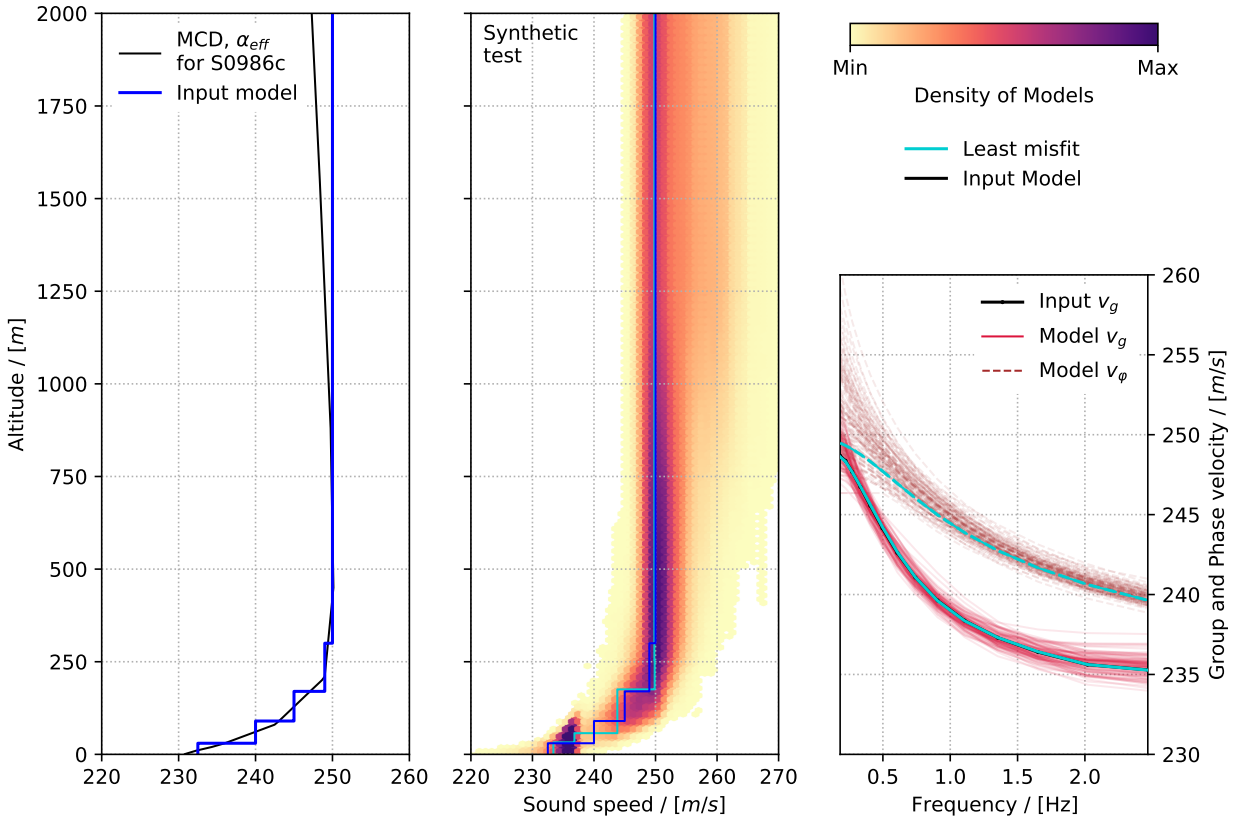

Figure S4. Result of a synthetic test of the McMC inversion. The input atmospheric model is a 4-layer simplification of the MCD effective sound speed profile for event s0986c (left). The associated synthetic group velocity curve is shown on the right in plain black line, among 100 group velocity and phase velocity curves extracted from the posterior distribution. The PDF of posterior models and least-misfit model (middle plot) both show a good agreement with the input model.

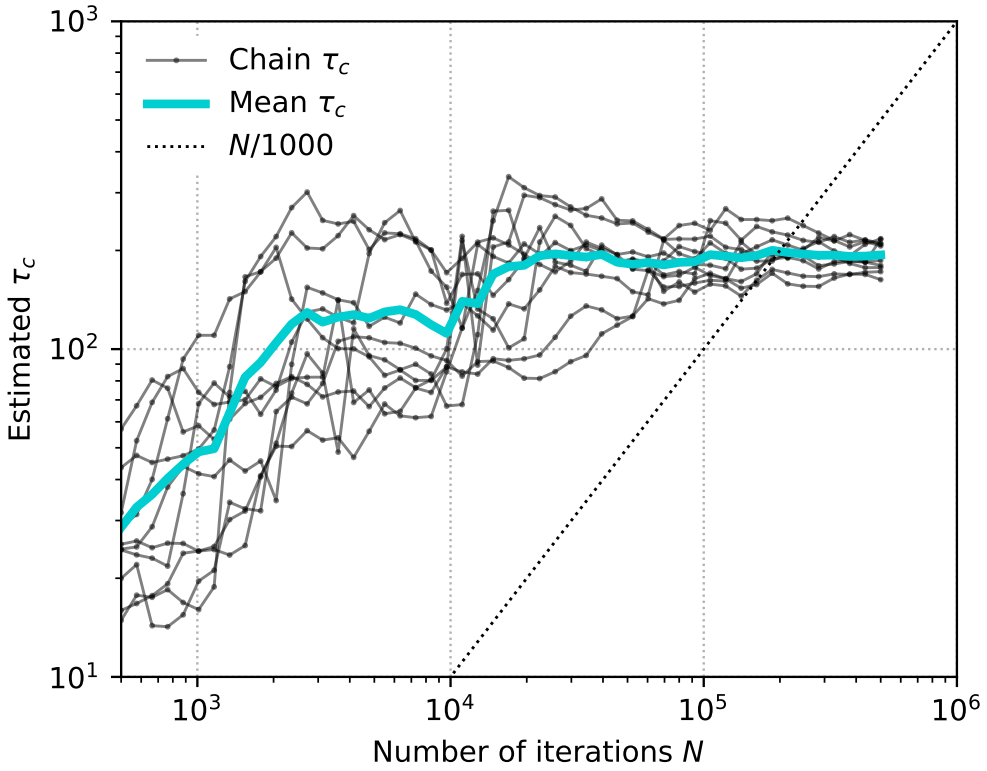

Figure S5. Test of the convergence of the synthetic McMC inversion. 10 Markov chains are run in parallel. The auto-correlation time τ_c of each chain is estimated from the chain of one chosen parameter (here α_0, the effective sound speed at the surface) as the simulation advances in steps N. Black lines show the variation of τ_c for each chain and the plain blue line is the mean τ_c estimated from the 10 chains. The chain is shown to reach convergence after about $N = 2 \cdot 10^5$ iterations and has an auto-correlation time of $\tau_c = 300$.

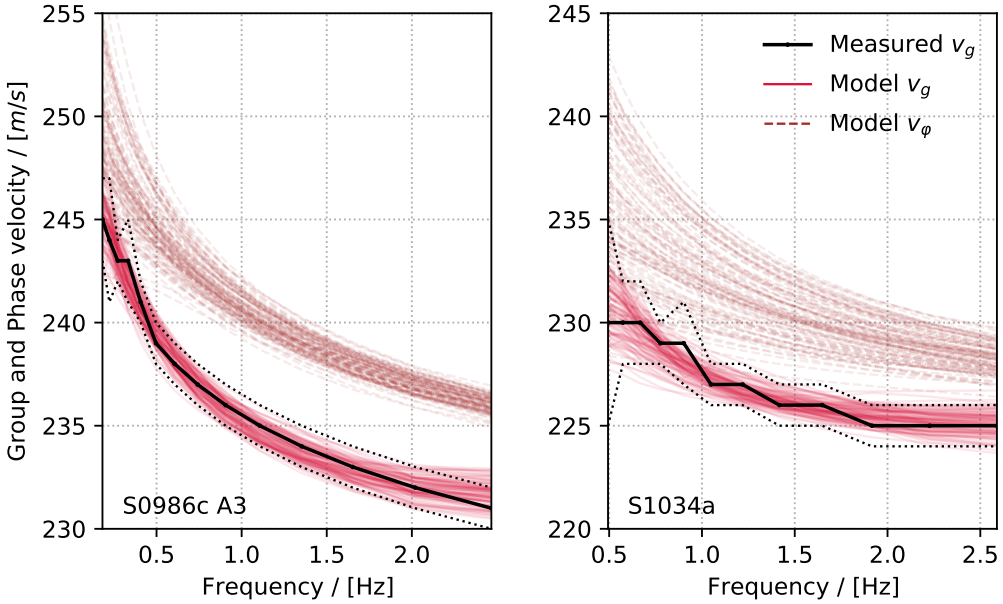

Figure S6. 100 group and phase velocity curves calculated from the posterior distribution of S0986c and S1034a. Measured group velocities are shown with their uncertainty in black.

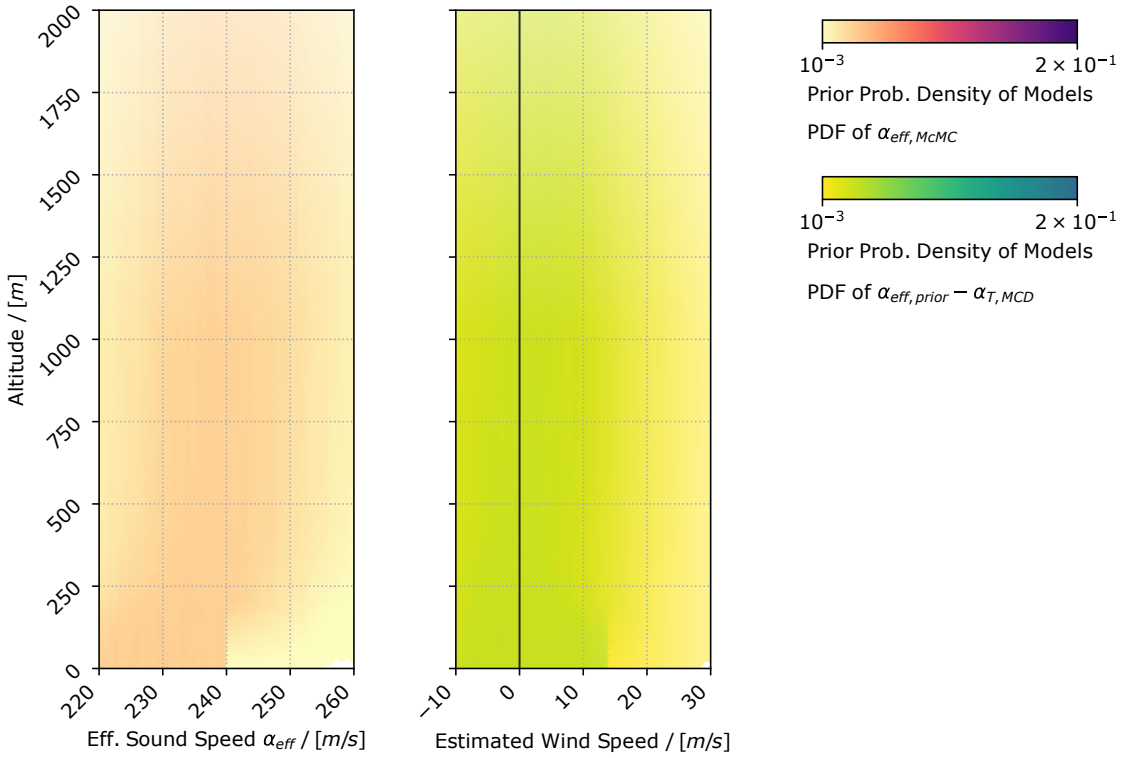

Figure S7. Prior PDF of effective sound speed and estimated wind speed models. The PDF is reconstituted by drawing 50,000 models randomly from within the prior bounds.

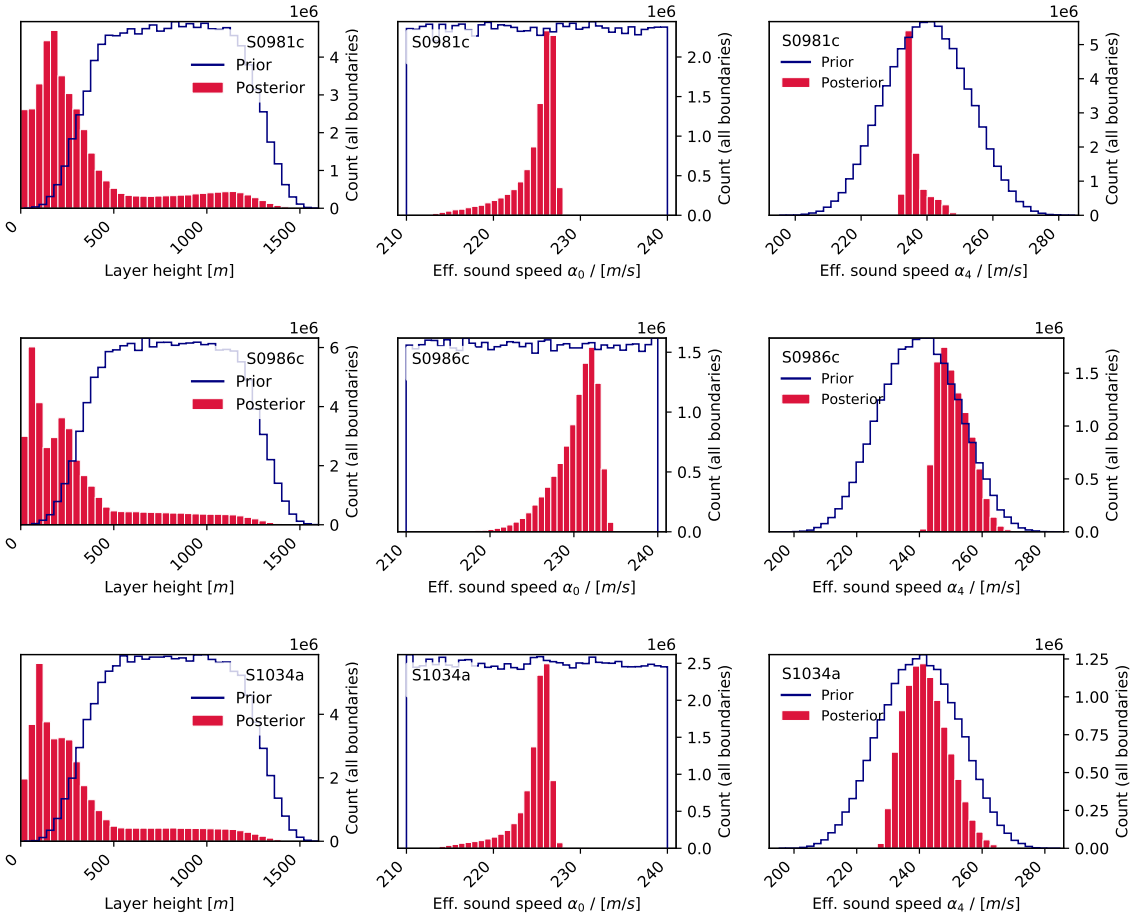

Figure S8. Histogram of parameter values extracted from the prior (blue line) and posterior (red bars) distributions for S0981c, S0986c and S1034a. The first column corresponds to combine height of all layers, $\{z_n\}$, the second to parameter α_0, i.e., the surface sound speed and the last to parameter α_4, i.e., the halfspace sound speed.

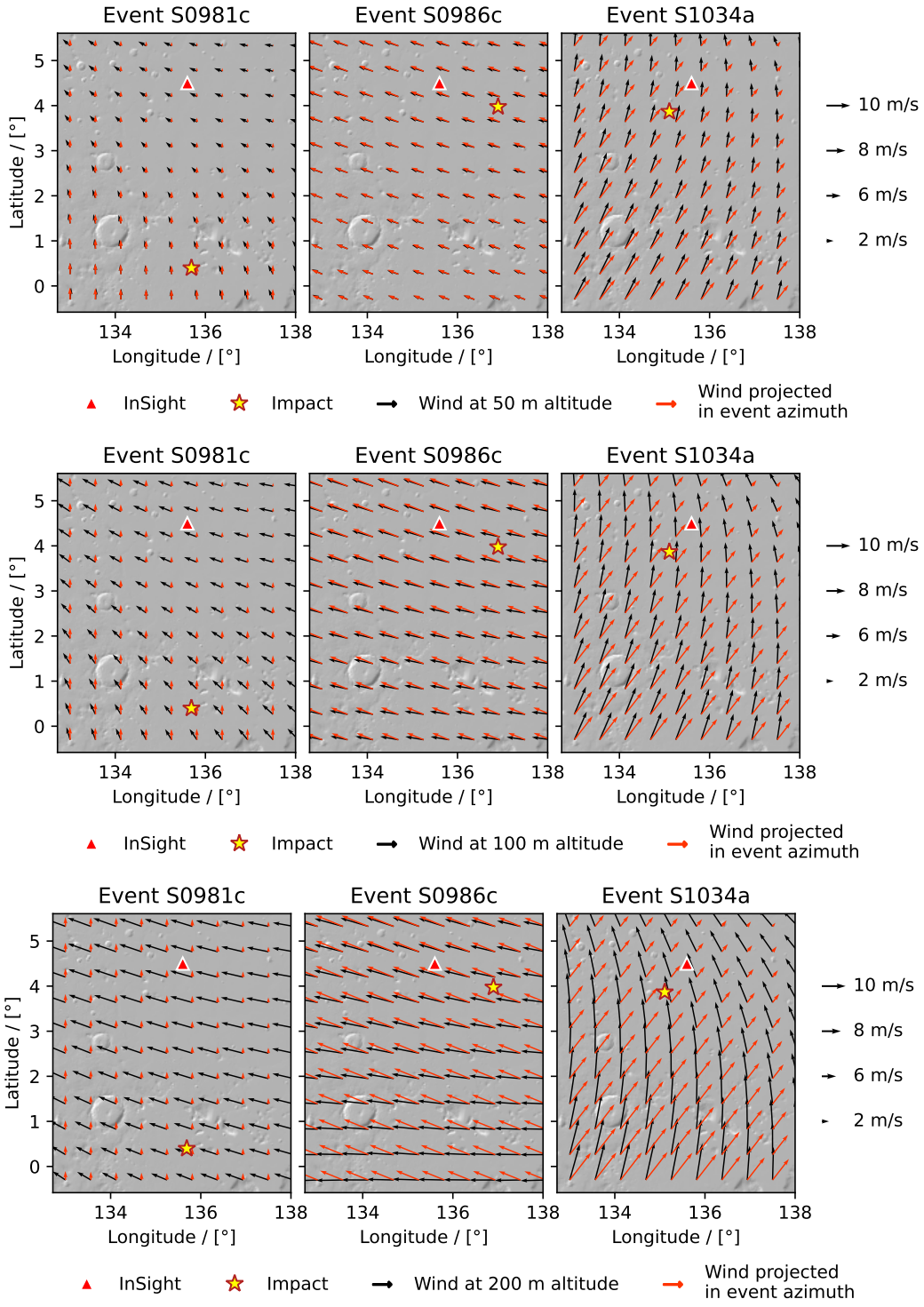

Figure S9. Map of the wind predicted by the MCD around InSight at the time of events S0981c, S0986c and S1034a at 50 m, 100 m and 200 m altitude. The projection of the wind in the impact→receiver direction is also displayed. The width and height of the map correspond roughly to the resolution in longitude and latitude of the grids used in the MCD interpolation.

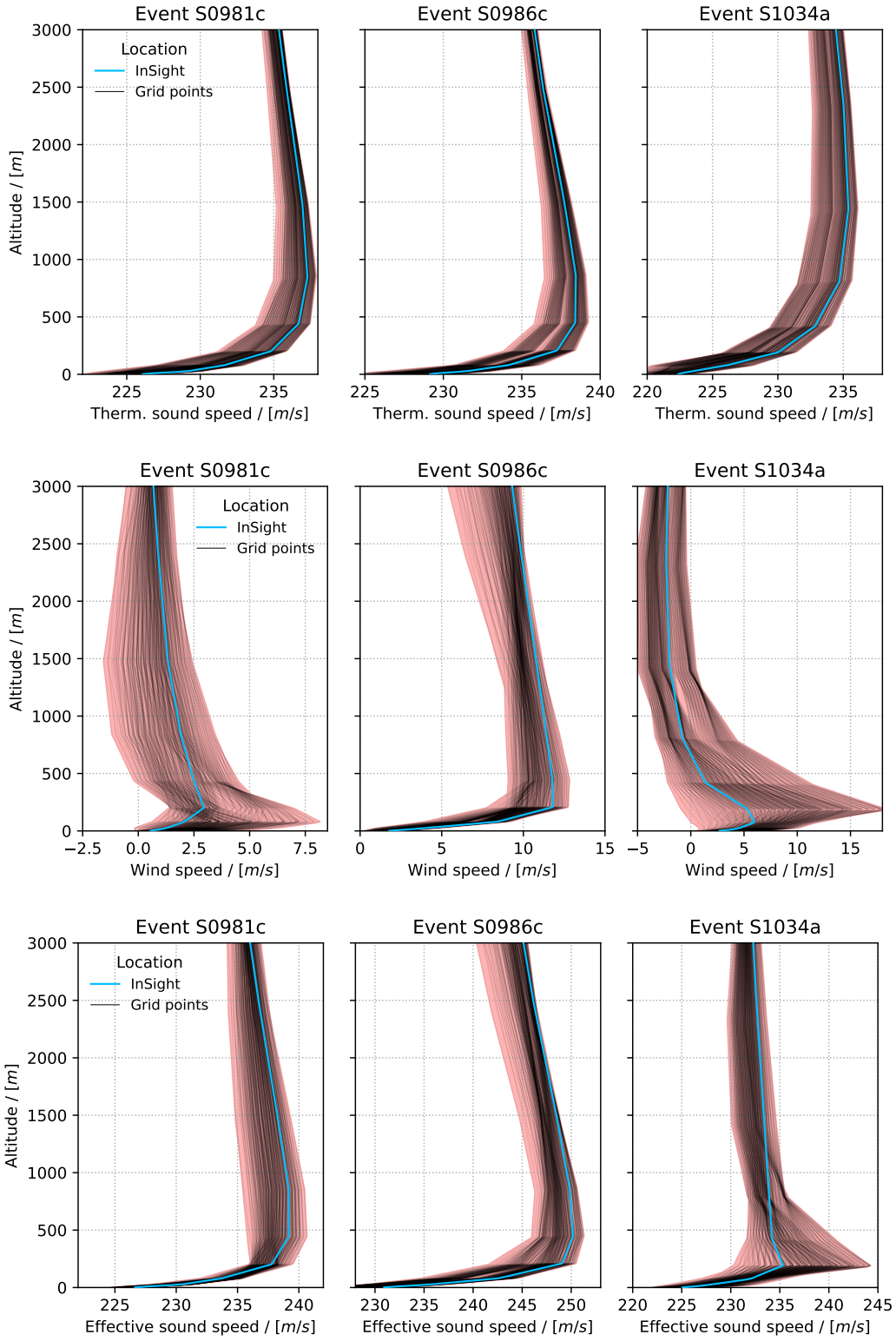

Figure S10. Profiles of thermodynamic sound speed $\alpha_T(z)$, winds $w_{\text{baz}}(z)$ in the impact→receiver direction and effective sound speed $\alpha_{\text{eff}}(z)$ calculated by the MCD. The profile at InSight location is given by a plain blue line. The profiles recorded at all other locations in the grid of Fig. S9 from one hour before to one hour after the event give a minimum and maximum bound to this estimated profile.